CLM-P312

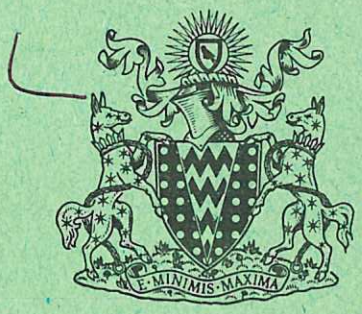

UKAEA RESEARCH GROUP

Preprint

A STUDY OF THE ION BEAM INTENSITY AND DIVERGENCE OBTAINED FROM A SINGLE APERTURE THREE ELECTRODE EXTRACTION SYSTEM

J R COUPLAND
T S GREEN
D P HAMMOND
A C RIVIERE

CULHAM LABORATORY
Abingdon Berkshire

1972

CLM-P 312

A STUDY OF THE ION BEAM INTENSITY AND DIVERGENCE OBTAINED FROM A SINGLE APERTURE THREE ELECTRODE EXTRACTION SYSTEM

J.R. Coupland, T.S. Green, D.P. Hammond and A.C. Riviere

(To be submitted for publication in Nuclear Fusion)

ABSTRACT

Experimental results are given for the perveance and beam divergence of a single aperture three electrode extraction system using helium ions at energies between 10 and 30 keV. The aperture radii, the electrode thicknesses and the spacings were varied and from the results a preferred design was obtained for use in a multi-aperture array. The most critical parameter was the ratio (S) of the radius of the first aperture to the distance between the first and second electrodes, the highest current density being obtained at values of this ratio less than 0.5.

The optimum beam divergence observed corresponded to a gaussian beam profile with a width (ω) of $\pm$ 1.2^{o} at 2 m from the source.

The measured perveance at small values of S and at minimum ω lay between 75 and 90 per cent of the value predicted on the basis of a simple model using the Langmuir Blodgett formula for the spherical diode.

U.K.A.E.A. Research Group
Culham Laboratory
ABINGDON
Berks.

September 1972

1. INTRODUCTION

Ion sources using arrays of circular apertures in their extraction electrodes are now used in several laboratories to obtain low divergence beams ($\pm$ 1° to 3°) of many amperes[1,2,3]. These are of particular interest to fusion experiments at the present time[4,5,6]. There is evidence that the performance of these multi-aperture sources is given by that of a single aperture multiplied by the number of apertures[7]. The aim of the present work was to determine the optimum design for a single aperture system for use in future multi-aperture sources. Measurements of the beam current and the beam divergence were made as a function of the aperture sizes, the electrode spacing and the electrode thicknesses. The most critical parameter was the ratio of the first aperture radius to the distance between the first and second electrodes. We call this ratio $S(= r_1/d_1$, Fig.2). The maximum current density was obtained for values of S less than $\approx$ 0.5. The other parameters, that is, the radius of the other apertures, the second gap separation and the electrode thicknesses, were found to be not so critical.

Earlier measurements on the extraction of an ion beam from a plasma by Harrison[8] were also made for a range of aperture radii and electrode spacings. His results showed good agreement with predictions based on the analytic treatment of the spherical diode by Langmuir and Blodgett[9]. However, the beam current was measured within a rather large angle of about $\pm$ 16° and for this reason his results are not directly applicable to the present purpose. The beam current within $\pm$ 2° from a single aperture system was studied by Hamilton et al.[10] but for rather large values of S (between 1.3 and 2.1). In the present work values of S between 0.28 and

1.33 were used. This was a continuation of the work of Coupland et al.[11] who used $1.0 < S < 3.0$, but was particularly stimulated by the high current density obtained by Cooper et al.[7] who used a specially shaped electrode and $S = 0.38$. Our results show that most of their improved performance was due to the small value of S.

Before describing the experimental system and presenting the results we give a simple analytic model for the ion optics of the extraction system.

2. BEAM DIVERGENCE AND THE EXTRACTION OPTICS

The ion optics of the extraction electrode system can be analysed in the same way as the optics of electron guns has been by Pierce[12] (see also Brewer[13]). In a simple idealised model one can consider that the total beam divergence is the sum of two effects. Firstly, the ions are emitted from a curved plasma boundary and collected on a curved extraction electrode, as a result the ions converge towards this electrode. Secondly, the ions diverge as they pass through the aperture in the extraction electrode, this aperture being an electrostatic lens.

The relationship between the plasma boundary curvature and hence initial convergence and the ion current is taken to be that given by Langmuir and Blodgett[9] for electron flow between spherical electrodes. Some experimental evidence for the validity of this was obtained by Harrison[8]. One should note that in the electron case the curvature is fixed and the Langmuir-Blodgett relationship enables one to calculate the space charge limited current. In the ion case the ion saturation current is fixed by the plasma parameters and the relationship now enables one to calculate the curvature of the

emitting boundary and hence the convergence for that current.

The divergence of the beam caused by the lens effect at the second aperture can be estimated from the thin lens formula derived by Davisson and Calbick[14]. Both the convergence and divergence can be related to the beam perveance $P = (I/V^{3/2}).(A/z)^{\frac{1}{2}}$ (cf. Appendix II) The net beam divergence can then be written as

$$\omega = 0.27\ S \left[1 - 2.25\ P/P_o \right] \text{ radians} \qquad \ldots (1)$$

where $S = r_1/d_1$ as above, and P_o is the perveance for plane parallel electrodes from the Child Langmuir law[15]

$$P_o = 1.72 \times 10^{-7}\ S^2 = (I/V^{3/2})\ (A/z)^{\frac{1}{2}} \text{ Amp Volt}^{-3/2} \qquad \ldots (2)$$

Equation (1) predicts that the divergence can be reduced to zero at a perveance equal to $0.44\ P_o$. That is, in this ideal system a plasma density can be found that will result in the formation of a parallel beam of ions. In practice the divergence does not decrease to zero and the perveance at the minimum divergence is less than $0.44\ P_o$. The factors which determine the residual divergence and the perveance are:

(I) Optical aberrations in the beam forming system due to:

- (a) distortion of the plasma boundary due to the use of plane electrodes of finite thickness;
- (b) non-uniformity of plasma density across the electrode aperture;
- (c) distortion of the field at the plasma due to the aperture in the second electrode; and
- (d) aberrations in the electrostatic lens of the second electrode aperture;

(II) Finite temperature of ions at the plasma boundary giving a finite transverse energy,

(III) Fluctuations in the beam intensity, and

(IV) Space charge expansion after extraction.

Clearly decoupling the two phases of motion in the analysis is a gross over-simplification which can introduce errors in the estimation of the perveance for minimum divergence, particularly at high S values.

The study of space charge expansion (Section 4) shows that it produces a measurable but small effect under our conditions. The residual divergence is believed to be due largely to I and II (cf. Section 5.4) with a small contribution from III.

3. EXPERIMENTAL SYSTEM

3.1 Plasma Source and Electrode Structure

The plasma source and electrode support structure were similar to those used by Coupland et al.[11] whose source was based on the duopigatron of Morgan et al.[16]. Several small alterations were made however and a schematic diagram of the actual source is shown in Fig.1. In the discharge region the internal diameter of the compressor electrode was increased to 2 cm and that of the anode to 3.2 cm. A modification was made also to the electrode insulators. The source operated under D.C. conditions without overheating and produced sufficient plasma for these single aperture measurements.

3.2 Plasma Density Control

The plasma density depended to some extent on all the parameters of the source. The magnetic field due to the coil on the compressor electrode and the arc voltage were set to fixed values which were optimum but not critical. The gas flow rate was set to a constant value which depended only on the electrode aperture size. Thus changes in plasma density required to optimise the beam current were

achieved by adjusting either the filament temperature, and thereby the arc current, or the magnetic field at the anode. Over some ranges of these two parameters they were interchangeable, a reduction in arc current requiring an increase in magnetic field. Above a certain field strength the source performance deteriorated, and although the total ion current decreased only slightly there was an appreciable increase in beam divergence. The magnetic field strength at the electrodes was $\sim$ 130 gauss and was too small to explain the increase in divergence by means of Busch's theorem[17]. The cause of the effect was not resolved and all the results presented here were obtained with the anode field below the critical value.

3.3 Electrode System

The beam forming electrodes were made of copper and were arranged as shown in Fig.2. The first electrode, which was at the plasma boundary, was operated at the potential V^+ corresponding to the desired beam energy. In the present measurements this ranged from 10 to 30 kV. The second electrode was held at a negative potential V^- which prevented electrons from leaving the beam plasma and which was adjusted to the minimum value consistent with maximum beam current. Further discussion on the effects of varying V^- is given in Section 5. The third electrode was held at ground potential. Current flowing to all three electrodes was metered. Under optimum conditions only a small fraction of the ion beam ($\sim$0.05) was intercepted on the second electrode giving rise to secondary electrons. Computed electric field plots showed that most of such secondaries would be accelerated back through the aperture in the first electrode. In the present energy range the secondary emission coefficient was expected to be between

1 and 2 so that with sufficient accuracy the total ion current leaving the source was calculated by subtracting the current to the second electrode from that to the first electrode.

3.4 Beam Ion Species

With hydrogen as a source gas H_1^+, H_2^+ and H_3^+ ions were produced whose relative intensities were a function of gas pressure and plasma density. Since our aim was to study the performance of the electrode system the complication of a varying ion mass was avoided by using helium. The discharge was also easier to operate with helium than with hydrogen. Mass analysis of the ion beam was carried out and this showed that the intensity of the He^{++} component was less than one per cent of that of the He^+ ion. The total intensity of heavier impurity ions ($4 \leq A < 25$) was between one and ten per cent of the total ion current.

3.5 Beam Flight Path and Measuring Equipment

The beam flight path and pumping system are shown in Fig.3. No focussing of the beam was used beyond that supplied by the electrode system. The beam current was measured on three concentric calorimeters which subtended maximum angles of $\pm 1.25^o$, $\pm 2.75^o$ and $\pm 10^o$ at the source exit aperture. The alignment of the beam with this system was checked regularly with two scanning probes, one operating along a vertical line and one horizontally at the positions shown. A beam profile recorded from a vertical scan is shown in Fig.4. Points calculated by assuming a Gaussian intensity distribution in angle normalised to the peak height are also shown. The points fit the results very well so for convenience a Gaussian distribution was assumed to hold for all the beam measurements. This seemed reasonable

from regular inspection of the profiles. By using the ratio of currents to the $\pm$ 1.25° and $\pm$ 2.75° calorimeters an angular width, $\pm \omega$, in degrees was calculated and used as a measure of beam divergence. This procedure was similar to that used by Cooper et al[7] but it assumes the beam is aligned with the centre of the calorimeter. Accurate machining and careful assembly of the electrodes was found to be necessary to ensure alignment to within $\pm$ 0.26° which was the maximum alignment error allowed during the measurements. By displacing a Gaussian profile across the detector system this is readily shown to give an overestimate of less than 0.05° in the value of ω. The total ion current leaving the source was accounted for by the beam measured on the calorimeters in all cases except when the maximum available beam within $\pm$ 10° was being determined. A significant fraction of the beam then lay outside $\pm$ 10°.

4. SPACE CHARGE EXPANSION OF THE BEAM IN FLIGHT

The beam divergence was found to decrease appreciably when the density of the background gas in the flight path was increased by letting in air. As shown in Fig.5 at 2.10^{-5} torr ω = 1.5°, but at 2.10^{-4} torr ω = 1.2° and at higher pressures ω increased again. Increasing the flow of gas from the source had a similar effect. This reduction in ω suggested an improved neutralisation of the space charge of the beam and to check this the associated changes expected in the actual ion trajectories were measured.

Two slits each 0.005 cm wide were used in conjunction with a movable probe 0.033 cm in diameter in the arrangement shown in Fig.6. The two trajectories established by the slits and probe were projected back to their apparent source point and the movement of this

point with gas pressure is shown in Fig.7 for a 20 keV He^+ beam. It can be seen that the apparent source lay close to the electrode system for all pressures indicating a high degree of space charge neutralisation. Also, the source point moved further from the measuring point as the pressure increased as would be expected for a reduction in space charge expansion.

Integration of the paraxial equation of motion of an ion in the beam allows one to calculate the possible values of the initial beam radius r_o, the initial beam angle θ_i and effective beam current I' which make the final beam radius and angle fit the measured values. The residual space charge fraction $\varepsilon = \frac{I'}{I}$ was assumed to be constant along the path and the electric field was calculated assuming cylindrical symmetry for the charge density. Within acceptable limits the values of ε and θ_i were found to be independent of r_o. A good fit to the observations required $\varepsilon = 0.015$ at 2×10^{-5} torr, and $\varepsilon = 0.005$ at 2×10^{-4} torr with $\theta_i \approx 0.9^o$ in both cases. These values of ε were than applied to the results of Fig.5 and a good fit was possible to the observed change in ω when $\theta_i = 1.0^o$. Comparison of this θ_i with the observed ω of 1.2^o shows that at 2×10^{-4} torr most of the observed beam divergence was present as the beam left the source. All the measurements were then made at this pressure. Cooper et al.[7] also made beam measurements in the presence of a high background gas density. A discussion of the collision processes occurring in the beam is given in Appendix I.

5. RESULTS

5.1 Change of Beam Divergence with Perveance

A general feature of the operation of the ion source, which is shown by equation (1), is the dependence of the beam current on the

angular acceptance of the measuring device. This is illustrated by the results shown in Fig.8. The beam current within the indicated angles is plotted as a function of arc current (and therefore plasma density) while keeping all other parameters constant. The maximum beam available within $\pm$ 2.75^{o} was greater than that within $\pm$ 1.25^{o} and was obtained at a higher plasma density. As the acceptance angle was increased less focussing was required by the curvature of the plasma boundary and the boundary moved forward because of the higher plasma density. The forward movement led to an increase in electric field strength and with the highest density an increased beam current resulted. Two points arise from this behaviour. Firstly, when comparing the performance of two sources the acceptance of the measuring device used for optimisation must be well specified. Secondly, if the acceptance angle can be increased then the beam current available will be larger, although not the current density (or beam brightness). A measure of beam brightness is P/ω^2 and from (1) this is seen to decrease with P for values of P above that for minimum divergence. In some applications the acceptance angle can be increased by the use of a lens, but use of a lens with multi-aperture sources is more or less excluded since the high gas flow causes charge exchange to occur close to the source. The data presented here have been recorded for maximum beam within $\pm$ 1.25^{o}, $I_{1.25}$, unless stated otherwise.

The currents to the second and third electrodes and the value of ω are also plotted in Fig.8 as a function of arc current. The increase in electrode loading at high arc currents indicates the increasing interception of the periphery of the ion beam as the beam divergence increased. At even higher currents than shown the source became difficult to control, the plasma apparently overcame the

applied field and a short circuit was formed between the first and second electrodes. The minimum value of ω, approximately 1.2^{o}, not surprisingly occurred at the arc current for maximum $I_{1.25}$. The values of ω are plotted as a function of perveance $I_T/V_T^{3/2}$ in Fig. 9 curve (a) where I_T is the total ion current and V_T is defined below. Also plotted, curve (b), are values of ω obtained by varying V^+ while keeping all other parameters constant and also the net ω predicted by equation (1). The latter refers to the total width of the idealised beam and not to a Gaussian half width. The agreement between the predicted P for minimum ω and the experimental values is remarkably good. The variation of ω with P is not so easy to compare because of the difference in the ω values described above. The effect of this rate of change of ω with arc current on the permissible variation of plasma density across a multi-aperture source is discussed in Appendix III.

5.2 Variation of Aspect Ratio $S = r_1/d_1$

The space charge limited current for a plane diode with an area the size of the first electrode aperture, πr_1^2, becomes from (2)

$$I = 8.6 \times 10^{-8} S^2 V_T^{3/2} \quad \text{Amp.} \qquad \ldots (3)$$

where $V_T = |V^-| + V^+$ for this electrode system and He^+ ions are assumed. At minimum divergence equation (1) predicts a value 0.44 times this for a concave plasma surface.

The presence of the second aperture and the thickness of the electrodes make the actual I less than that given by (1) by an amount which depends on S. This is illustrated by the results shown in Fig. 10. The beam currents obtained at 20 keV are plotted as a function of S for optimisation within $\pm 1.25^{o}$, $\pm 2.75^{o}$ and $\pm 10^{o}$

together with the plane diode result from equation (3). Hamilton et al.[10] gave results for S = 1.3, 1.7 and 2.0 at a fixed d_1 and for optimisation within $\pm 2^0$. A mixed beam of hydrogen and deuterium ions was used and if a mean ion mass of 2 is assumed then their results are in good agreement with those of Fig. 10 (a).

At high S values the currents fall below those predicted by an S^2 law. Kelley et al.[18] reported that their beam current varied as $\left(\frac{S}{1+S}\right)^2$ although no results were given. Here the data are better fitted by the relationship

$$I \propto \frac{S^2}{1 + aS^2} \quad . \qquad \ldots (4)$$

The solid curves drawn in Fig.10(a) are based on this relation with a = 3, 3.3 and 2.2 for the $\pm 1.25^0$, $\pm 2.75^0$ and $\pm 10^0$ cases respectively. The differences between these values of a are probably not significant for the present data since the critical value for S varies as $a^{-\frac{1}{2}}$. It can be seen that the current within $\pm 10^0$ approached to within a factor of 2 to that of the plane diode equation (3) at small S. The total ion current in the case $\pm 10^0$, S = 0.31 was within 5 per cent of that expected from (3).

By dividing the observed I by πS^2 one obtains the current density correctly scaled for different d_1 and it is readily found that the maximum current density and therefore beam brightness is obtained at small S. This behaviour leads directly to the use of multi-aperture arrays for high current low divergence sources. If the total electrode area is πR^2 and the number of apertures N then, with a packing fraction $P = Nr_1^2/R^2$, we may write $S = \frac{R}{d_1}\left(\frac{P}{N}\right)^{\frac{1}{2}}$. From Fig.10(a) and (4) we see that the maximum current density is reached for $S \ll a^{-\frac{1}{2}}$. For d_1 fixed by the breakdown limit this can be achieved by using a large N. There is a practical limit to N

however, through the thermal limitations discussed by Cole et al.[19], since, as will be seen below, the thickness of the first electrode must scale as r_1. For small R it eventually becomes more worthwhile to use a single aperture and large S.

5.3 Variation of Scale Size

Both equations (1) and (2) show that the beam current should be independent of the scale size of the electrodes. Results obtained with the present source for S = 0.38 and r_1 = 1, 2 and 3 mm are shown in Fig.11. For these results all electrode spacings and thicknesses were scaled with r_1 except for the case r_1 = 3 mm when D_2 and D_3 were left equal to the values used for the r_1 = 2 mm case. Both the total ion current and $I_{1.25}$ decreased by 10 to 15 per cent as r_1 changed from 1 to 3 mm, whereas ω improved from 1.3^{o} to 1.1^{o}. These changes are small and the performance is independent of scale size to first order. The small changes could be explained by a narrow radial distribution of plasma density. However the plasma density required for the 3 mm scale is nine times less than that required for the 1 mm scale and a change in transverse ion temperature is also plausible. For both r_1 = 2 and 3 mm the variation of I with S was the same, as is shown by the results in Fig.10(a). The corresponding measurements for differing S were not made for r_1 = 1 mm.

5.4 Variation of Beam Energy E

Equation (2) also predicts a variation of optimised current as $V_T^{3/2}$. Results for beam current and ω as a function of beam energy $E(= V^+)$ are shown in Fig.12 for $\left|\frac{V^-}{V^+}\right| = 0.1$. The total ion current varied closely as $E^{3/2}$ as expected for fixed $\frac{V^-}{V^+}$. The decrease in ω with E was not as fast as would be expected if the beam divergence

were solely due to a fixed transverse ion temperature at the plasma surface when ω would vary as $E^{-\frac{1}{2}}$. The dotted line marked $\omega \propto E^{-\frac{1}{2}}$ in Fig. 12 assumes a transverse ion temperature of about 7 eV. However if the divergence were due solely to optical aberrations then ω would be independent of E. The value of ω is perhaps a combination of these two effects as suggested by Septier and Osher[20].

5.5 Variation of the Ratio of Aperture Radii, r_2/r_1

Since the departure from $I \propto S^2$ is possibly due to the presence of the second aperture, it is of interest to vary the ratio of r_2/r_1. For large d_1 (small S) the radius of the second aperture would not be expected to have much influence unless aberration due to the lens effect at this electrode was important in determining ω. The results obtained for several values of r_2/r_1 are shown for S = 1.33 and 0.38 in Figs.13 and 14 respectively. In neither case however, were $I_{1.25}$ or ω sensitive to this parameter in the range of values tried. From Figs.13 and 14 it is deduced that the variation with S shown in Fig. 10(a) is not sensitive to changes in r_2/r_1. The advantage in using $r_2/r_1 > 0.75$ can be seen by the reduction in the current drain and therefore thermal loading to the second electrode which arises because of impact by the beam.

5.6 Variation of Aperture Radius r_3 in Third Electrode

The effect of varying r_3 as r_1 and r_2 were kept fixed is shown in Fig.15 for S = 0.38. Again $I_{1.25}$ and ω showed little dependence on r_3, but the current drain fell as r_3 increased. In this case the current to the electrode probably included a net current due to the flow of ions and electrons from the beam plasma. The 2 mA which appears to be independent of r_3 could represent this net current and the increase to 3 mA at $r_3 = 1.4$ the result of beam

hitting the electrode. This measurement of beam interception was enhanced possibly by a large secondary emission coefficient arising because of grazing incidence of the ions. This must be allowed for in deducing the actual thermal loading[19].

5.7 Variation of Second Gap Length, d_2 and Thickness of Second Electrode, D_2

Results obtained by changing d_2 while keeping all other dimensions fixed are shown in Fig.16. Here it is clear that lengthening the second gap worsened the performance by decreasing $I_{1.25}$ and increasing ω. A calculation of the space charge expansion of an initially parallel ion beam showed an increase in beam divergence of 0.5^{o} as d_2 increased from 0.4 to 4 mm. Although this result appears to explain the change in ω shown in Fig.16 the plasma density and therefore boundary curvature was re-optimised for each value of d_2 and an exact correlation is not possible. The results showed however that d_2 should be made as small as possible, consistent with avoiding vacuum breakdown due to the V^- potential. Similar conclusions are reached for the thickness of the second electrode, D_2. The effect of varying D_2 is shown by the results in Fig.17. The current, $I_{1.25}$, decreased, and the optimum ω and V^- increased as D_2 was increased so that the indication again is that the overall length of the second part of the electrode system should be kept short.

5.8 Variation of First Electrode Thickness, D_1

As discussed by Cole et al.[19] there are limitations to the beam current from a multi-aperture source due to thermal loading. The worst thermal problem is probably in the first electrode and this

might be alleviated by making the electrode thickness D_1 greater and thereby improving heat conduction and thermal capacity. Results obtained as a function of D_1 are shown in Fig.18 for constant values of the other dimensions. For small D_1 it appeared that a satisfactory plasma boundary shape was not possible with the result that the second and third electrode loadings and ω were high. An optimum value for ω appears to exist at about $D_1/r_1 = 0.5$. For larger D_1 the plasma loss to the walls of the aperture leads to an increased requirement for arc current.

5.9 Variation of V^-/V^+

The purpose of the negative electrode is to produce a potential barrier to the electrons which would otherwise be drained from the beam plasma by the source extraction field. The variation of the beam current at low values of V^-/V^+ is shown in Fig.19 where a marked improvement in transmitted current occurs above a critical potential. The actual potential on axis in the aperture is less than the applied value V^- because of field penetration. The vacuum field distribution was computed for the case $r_2 = r_3 = 0.7$ mm, $d_1 = 2.6$ mm, $d_2 = D_2 = 0.75$ mm and $D_3 = 1.4$ mm which has the same aspect ratios as that used for the experimental results. The calculated variation of the effective potential with the value of V^-/V^+ is shown in Fig. 20. The potential barrier is reduced by the space charge of the ions and for the present electrode performance this potential is of the order of 140 volts. This correction is plotted in Fig.20 and comparison of Figs.19 and 20 shows that the effective potential on axis is just going negative when the current had reached half the peak value.

It can be shown that altering the ratio V^-/V^+ changes the focussing effect of the second and third apertures. The net change in the angle of focussing can be calculated approximately as in Appendix II but with the additional effect of the third aperture

$$\Delta\theta = \frac{1}{3}\frac{r_b}{d_1}\left(1 + \frac{d_1}{d_2}\left(2 - \left(\left|\frac{V^-}{V^+}\right| + 1\right)^{-\frac{3}{4}} - \left(\left|\frac{V^-}{V^+}\right| + 1\right)^{\frac{3}{4}}\right)\right)$$

Here r_b is the mean beam radius through the electrodes. As $\left|\frac{V^-}{V^+}\right|$ changes from 0.1 to 1.0, $\Delta\theta$ decreases from $+4^o$ to 0^o so that the focussing required by the plasma boundary is substantially decreased.

Results for $I_{1.25}$ and ω at values of V^-/V^+ from 0.05 to 0.6 are shown in Fig.21 by the solid circles and broken curves. It can be seen that $I_{1.25}$ does not increase appreciably with V^-/V^+, as would be expected from the increase in perveance allowed, and ω worsens quite rapidly. There is evidence however that, at V^+ of 10 keV and V^-/V^+ greater than 1.4, ω decreases and $I_{1.25}$ increases with V^-/V^+.

5.10 Comparison with Electrode Design of Cooper et al.[7]

Cooper et al.[7] found that a higher beam brightness was achieved by forming a recess around the aperture in the first electrode as illustrated in Fig.22. The probable effect of the recess is shown by the computed equipotentials for the vacuum field in Fig. 23. The recess allows a more uniform curvature across the plasma boundary (or alternatively excludes plasma from the regions of excessive curvature at the edges of the aperture). Results obtained with the recessed first electrode are shown in Fig.21 with the results of the non-recessed electrode. For these measurements S = 0.38 and was close to the value used by Cooper et al.[7]. A particular feature of the recessed electrode design is revealed by these results. $I_{1.25}$

increased almost as $V_T^{3/2}$ with ω nearly constant whereas with the straight hole $I_{1.25}$ increased only slightly and ω worsened rapidly.

It is possible that the aberrations of the plasma surface are a stronger function of its curvature in the non-recessed case and any departure from the optimum leads to an increase in ω.

It is important to note that in this parameter range the recessed electrode allows one to vary the extracted beam current at constant beam energy by varying V^- but maintaining the final beam energy constant without degradation of beam divergence. This behaviour of the recessed electrode system was not found at S = 1.33, but rather the reverse.

At small V^-/V^+, $I_{1.25}$ for the recessed system was 50 per cent greater than for the non-recessed and ω was 1^o showing that the modified electrode allows a very high quality beam to be produced. For multi-aperture systems however, there is a disadvantage in using the recessed electrode since the overall space required for a single aperture is increased by 70 per cent and there is an additional problem of thermal loading on the thin edge. For these reasons the straight hole is believed to be the better choice for multi-aperture sources unless flexibility of operating energy is of primary importance.

5.11 Voltage Breakdown Across First Gap

Equation (1) shows that the beam current is inversely proportional to the electrode separation d_1. There is a limit to how small d_1 can be made due to breakdown by the potential V_T. The values of V_T at which some trouble with breakdown was experienced while operating the source at various values of d_1 are shown in Fig.24. The solid curve assumes $V_B = Bd^{\frac{1}{2}}$ with $B = 6 \times 10^4$ V cm$^{-\frac{1}{2}}$ and this appears to be a reasonable fit to the data.

6. SUMMARY

The results obtained have shown a clearly defined set of parameters for the electrode design of a single aperture in a multi-aperture array. The recommended values are given in Table I together with the performance to be expected. The degree of variation permitted for each parameter can be estimated from the results given in Section 5. The application to multi-aperture sources is discussed further by Cole et al.[21].

The good agreement obtained between experiment and theory for the optimisation of divergence and its variation with perveance suggests that the performance of these systems is now well understood. The reasons for the residual divergence at optimimum adjustment being about 1^{o} are not known and should lower divergences be required further investigation will be necessary.

7. ACKNOWLEDGEMENTS

The present work was a continuation of the program of ion source development started by E Thompson. The authors are also indebted to D R Sweetman for many helpful discussions, and would like to acknowledge E M Jones for his assistance with the computing and particularly F Watters for his help in the experimental measurements.

TABLE I

d_1	$2.8.10^{-10}.\ V_T^{\ 2}$ cm.volt^{-2}
r_1/d_1	0.4
r_2/r_1	1.0
D_1/r_1	0.5
r_3/r_2	1.0
$\frac{D_2}{D_1} = \frac{D_3}{D_1}$	1.2
$\frac{d_2}{r_2}$	0.5
$\frac{V^-}{V^+}$	0.05
minimum $\frac{\text{For 20 keV } He^+}{\omega}$	$1.2^o \pm 0.1^o$
I within $\pm 1.25^o$	7.8 ± 1 mA
I within $\pm 2.75^o$	16 ± 1 mA

APPENDIX I

Space Charge Neutralisation of Beam in Flight

In the flight path the beam ions ionize and capture electrons from the background gas molecules and also release secondary electrons from the metal surfaces. Although the probability for charge exchange over the 2 m path was about 0.45 most of the space charge expansion occurred during the first short section of path where the fraction of charge exchange events was small and the change in ω with gas pressure is not explained by charge exchange.

The average energy $\bar{E}$ of secondary electrons ejected by He^+ on molybdenum[22] and of electrons formed by ionization of He and H_2 by H^+ ions[23,24] are shown in Fig.AI.1. It is probable that the value of $\bar{E}$ is related to the velocity of the ion rather than its energy so that for 20 keV He^+ ions we would expect $\bar{E}$ to be approximately 7 eV from either source. The beam potential due to space charge corresponding to the value of ε obtained in Section 4 is about 1 volt. This is substantially smaller than $\bar{E}$ at 7 eV so that very few of the primary electrons would be electrostatically contained in the beam. The reduction in ω with increased gas pressure was most probably caused by more rapid trapping and cooling of electrons within the weak potential well.

Since we were concerned with the performance of the electrodes and were ultimately concerned with the production of beams of neutral atoms the need for high gas pressure to minimise ω was not considered a problem and further study of the effect was not pursued. A more detailed calculation of the residual beam potential to be expected has been made by Hamilton[25].

APPENDIX II

Ion Optics for Extraction System

1. Basic Theory

The extraction of an ion current from a plasma boundary depends on the applied electric field and the conditions in the plasma. A full analysis of ion dynamics and the plasma boundary conditions would be very complex; even recent numerical analysis using computers make certain simplifying assumptions. To obtain a qualitative understanding we adopt a simple approach, similar to that used to estimate the behaviour of electron guns (see, for example, Brewer[13], Pierce[12]).

In this analysis we first relate the curvature of the plasma boundary to the voltage and the saturated ion current density which can be extracted from the plasma

$$J_S = n_i\, e \left[\frac{k\, T_e}{M_i}\right]^{\frac{1}{2}} .$$

Secondly we calculate the variation of initial beam convergence θ with the plasma boundary curvature, and finally we estimate the lens effect of the aperture in the extraction electrode (Fig.II.1).

(a) Space charge limited flow between curved surfaces

The calculation of the space charge limited flow J_s between plane surfaces (Child-Langmuir[15] law) has been extended by Langmuir and Blodgett[9] to cover both spherical surfaces and cylindrical surfaces. For plane surfaces the current density J_s is related to the voltage by the equation

$$\frac{J_s}{V^{3/2}}\left(\frac{A}{z}\right)^{\frac{1}{2}} = P_{DO} = \frac{5{\cdot}5 \times 10^{-8}}{d^2} \text{ amp volt}^{-3/2}\ \text{cm}^{-2} \quad \ldots \text{(AII.1)}$$

where P_{DO} is the perveance per cm^2.

In the case of concentric spherical electrodes equation (AII.1) becomes

$$\frac{J_s}{V^{3/2}} \left(\frac{A}{z}\right)^{\frac{1}{2}} = \frac{5.5 \times 10^{-8}}{R_1^2 \alpha_1^2} \text{ amp. volt}^{-3/2} \text{ cm}^{-2} \quad \ldots \text{(AII.2)}$$

where $\alpha = Y - 0.3Y^2 + 0.075Y^3$

and $Y = \log_e \left[\frac{R_2}{R_1} \right]$

R_1 is radius of curvature of emitting surface, i.e. plasma

R_2 is radius of curvature of collecting surface, i.e. extractor

d is gap between the surfaces $(d = R_1 - R_2)$

V is applied voltage

A is the atomic mass and z is the charge of the ions.

Tabulated values of α are given in Brewer's article. For small values of $R_2 - R_1$ we can use the expansion for α and derive the approximate result

$$\frac{J_s}{V^{3/2}} \left(\frac{A}{z}\right)^{\frac{1}{2}} = \frac{5.5 \times 10^{-8}}{d^2} \left[1 - 1.67 \frac{d}{R_1}\right] \text{ amp. volt}^{-3/2} \text{ cm}^{-2} \quad \ldots \text{(AII.3)}$$

Equations (AII.2) and (AII.3) essentially relate the curvature of the emitting surface to the other parameters of the beam. If we write P_D as the density perveance of the beam at the plasma surface and P_{DO} as the value given by the Child-Langmuir law, equation (AII.1), then

$$R_1 \simeq 1.67 \frac{P_{DO}}{P_{DO} - P_D} \, d \, .$$

(b) Relation to currents through apertures and beam convergence

We can now consider the current flow from a small circular area of the spherical surface. The source has an aperture of radius r_1 and the beam is emitted within a conical section of half angle θ, Fig.AII.1. Therefore we have $R_1 = r_1/\sin\theta \simeq r_1/\theta$ and the total

current I is given by $I = \pi r_1^2 J_s$. Equation (AII.3) can be modified to

$$P_s = \frac{I}{V^{3/2}} \left(\frac{A}{z}\right)^{\frac{1}{2}} = 1.72 \times 10^{-7} \left(\frac{r_1}{d}\right)^2 \left[1 - 1.67 \frac{d}{r_1} \cdot \theta\right] \quad \ldots \text{(A.II.4)}$$

Here we see that the perveance of the hole depends on the square of the aspect ratio $S = r_1/d$ and also on the convergence angle θ. If we define θ geometrically by requiring that the beam just passes through an aperture r_2 in the extractor, then $\theta = \frac{r_1 - r_2}{d}$. The relationship between the perveance r_1, r_2 and d, thus derived, was confirmed by E. Harrison[8] some years ago.

(c) Lens effect of aperture in the extractor

The extractor separates two regions, one of longitudinal electric field almost equal to zero in the drift space and one of longitudinal field, E equal to $\frac{V}{D}$, in the accelerating gap. Between the regions there must be a transverse electric field and this causes the beam to diverge. The angle of divergence Ψ can be calculated from the first order equation derived by Davisson and Calbick[14] for the zero space charge case

$$\tan \Psi = \frac{E}{4V} r_2 = \frac{r_2}{4d} \quad ,$$

where r_2 is now the radius of the beam in the aperture.

Since the electric field in the accelerating gap is affected by space charge one finds that E is closer to $\frac{4}{3} \frac{V}{d}$ giving a value of $\tan \Psi$ of $\frac{r_2}{3d}$. One can obtain more accurate values of E taking into account the effect of the convergence of the beam[12,26]. Then one finds

$$\Psi \simeq \frac{r_1}{3d} \quad . \qquad \ldots \text{(AII.5)}$$

One can combine equations (AII.4) and (AII.5) to derive an expression

for the net divergence ω in terms of the working perveance P and the plane diode perveance P_o. The result is

$$\omega = \frac{4}{15} \frac{r_1}{d} \left[1 - \frac{9}{4} \frac{P}{P_o} \right] . \qquad \ldots \text{(AII.6)}$$

APPENDIX III

Effect of Plasma Density Variation on Beam Divergence from Multi-Aperture Sources.

The analysis given in Appendix II predicts, and experiments confirm, that it is possible to obtain a low divergence beam with a single aperture extractor system, by selecting the correct perveance. When using a multi-aperture extractor system across a large area plasma source, the perveance per aperture may vary across the source radius due to variation in plasma density. Thus whilst the perveance may be optimised to give low divergence at the centre, it may be far from optimum at the outer radii so that the divergence is increased at these radii. Whilst schemes have been proposed for shaping the multi-aperture electrodes to correct for this effect[27], we consider that one should first examine the limitations on operation which arise with plane electrodes.

To do this we use equation (AII.6) of Appendix II to relate the variation in divergence to the variation in perveance. Let us assume that the system is optimised for zero divergence at the centre, i.e. the perveance at the centre P_c equals 0.44 P_o. Then the divergence at the extreme radius is given by

$$\omega_e = 0.27 \frac{r}{d} \left[\frac{P_c - P_e}{P_c} \right] \quad \text{radians} .$$

Since $\frac{P_c - P_e}{P_e}$ is equal to $\frac{\Delta n}{n}$ across the source we have

$$\omega_e = 15.5 \frac{r}{d} \frac{\Delta n}{n} \quad \text{degrees} .$$

Thus if we can allow ω_e to be 1^o we can allow $\frac{r}{d} \frac{\Delta n}{n}$ to be 6.4×10^{-2}. In Fig.AIII.1 we plot the limiting values of $\frac{\Delta n}{n}$ against $\frac{r}{d}$ (equal to S) for ω_e to be less than 1^o, and 3^o.

Typically if we work with S equal to 1.0 we are limited to $\Delta n/n$ of 6.4% for $\omega < 1^{o}$ and 19.2% for $\omega < 3^{o}$. Alternatively we can state that if $\Delta n/n$ for a source is 20% then limiting ω to 3^{o} means that S must be less than 0.96.

REFERENCES

1. DAVIS, R.C. et al., Rev. Sci. Instr. 43, (2) pp.278-283 (1972).
2. OSHER, J.E. and HAMILTON, G.W., Symposium on Ion Sources and Formation of Ion Beams, Brookhaven Oct. 1971.
3. ALDCROFT, D., BURCHAM, J., COLE, H.C., COWLIN, M. and SHEFFIELD, J. Vth European Conf. on Controlled Fusion and Plasma Physics, Grenoble, August 1972.
4. SWEETMAN, D.R., et al, Proc. 4th Int. Conf. Plasma Phys. Controlled Nucl. Fusion Res., Madison, 1971 (I.A.E.A., Vienna 1971) Vol. III, pp. 393-408.
5. STIX, T H, Plasma Phys. 14, 367 (1972).
6. KELLEY, G.G., et al, Nuclear Fusion 12, pp. 169-175 (1972).
7. COOPER, W.S., et al, Nuclear Fusion 12, 263-265 (1972).
8. HARRISON, E.R., J. Appl. Phys. 29, 909 (1958).
9. LANGMUIR, I. and BLODGETT, K.R., Phys. Rev. 24, 49 (1924).
10. HAMILTON, G.W., HILTON, J.L. and LUCE, J.S., Plasma Phys. 10,687 (1968).
11. COUPLAND, J.R. and THOMPSON, E. Rev. Sci. Instr. 42, (7) pp.1034-1037. (1971).
12. PIERCE, J.R. Theory and Design of Electron Beams, Van Nostrand, Princeton (1949), pp.173.
13. BREWER, G.R. Focussing of Charged Particles II, (Ed. Septier) Academic Press (1967) , pp.23.
14. DAVISSON, C.J. and CALBICK, C.J. Phys. Rev. 38, 585 (1931).
15. CHILD, C.D., Phys. Rev. 32, 492 (1911).
    LANGMUIR, I., Phys. Rev. 2, 450 (1913).
16. MORGAN, O.B., KELLEY, G.G. and DAVIS, R.C., Rev. Sci. Instr. 38, 467, (1967).
17. KIRSTEIN, P.T., KINO, G.S., WATERS, W.E., Space Charge Flow. McGraw-Hill, New York p.15(1965)

18. KELLEY, G.G., LAZAR, N.J. and MORGAN, O.B., Nucl. Instr. and Methods, 10, 263 (1961).

19. COLE, H.C., HAMMOND, D.P., JONES, E.M., RIVIERE, A.C. and SHEFFIELD, J., Second Int. Conf. on Ion Sources, Vienna, September 1972.

20. SEPTIER, A., Symposium on Ion Sources and Formation of Ion Beams, Brookhaven, October 1971, BNL-503 Lo, pp.9-16.
OSHER, J.E., ibid. pp.137-144.

21. SHEFFIELD, J. et al, To be published.

22. WEHNER, G, Z. Physik V.193, p.439 (1966).

23. KUYATT, C.E. and JORGENSEN, T, Phys. Rev. 130 pp. 1444-1455 (1963).

24. RUDD, M.E. and JORGENSON, T, Phys. Rev. 131 pp. 666-675 (1963).

25. HAMILTON, G W. Private Communication (1971).

26. THOMPSON, E. Private Communication (1972).

27. Annual Progress Report Oak Ridge National Laboratory. Thermonuclear Division. ORNL-4688 p.92 (1970).

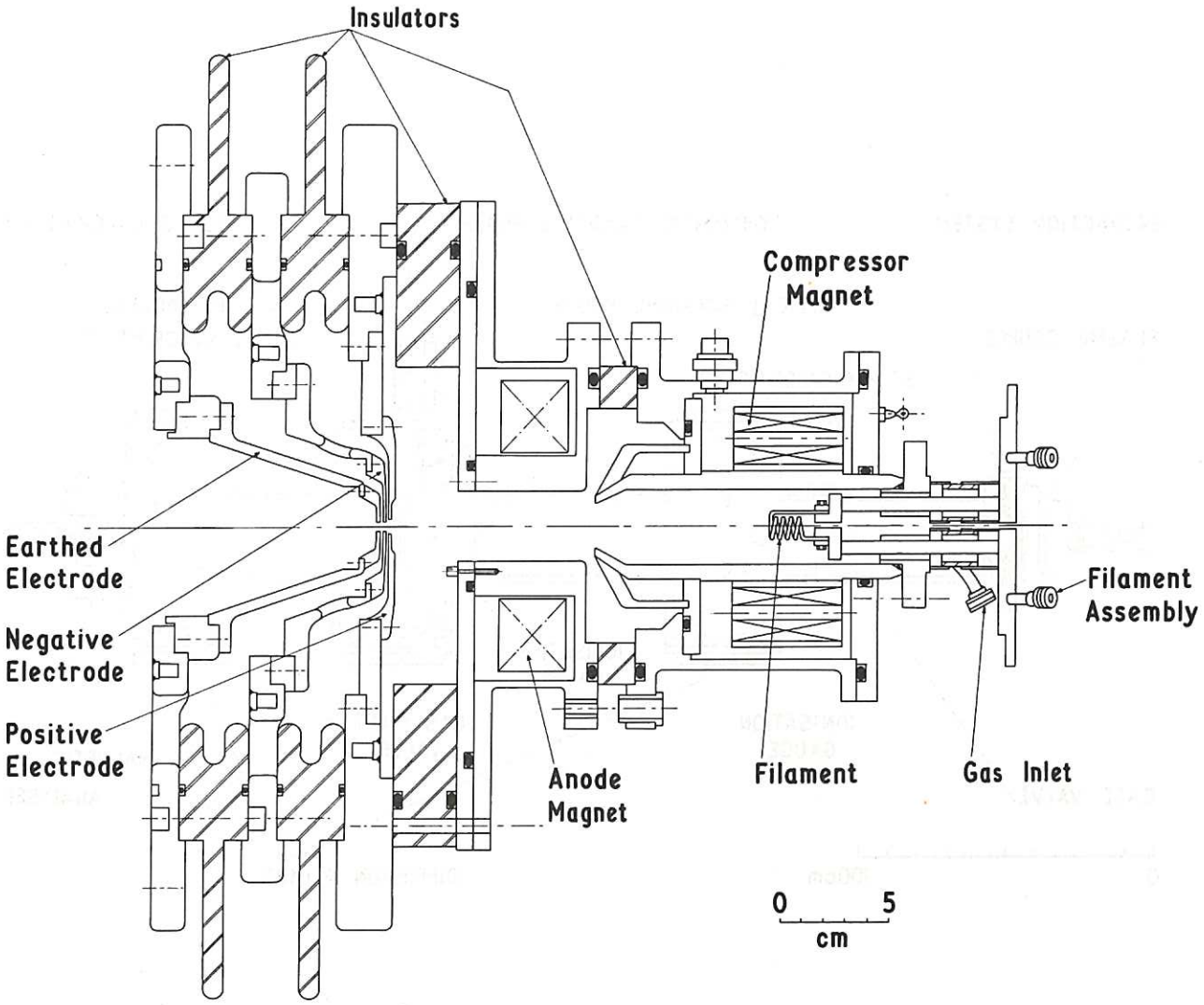

Fig.1 The ion source and electrode arrangement.

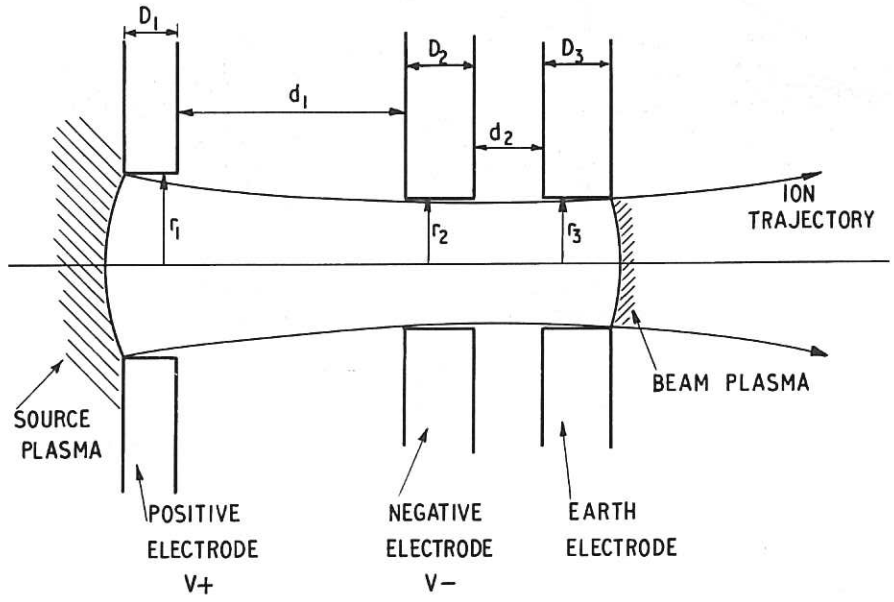

Fig.2 The single aperture electrode system which was studied.

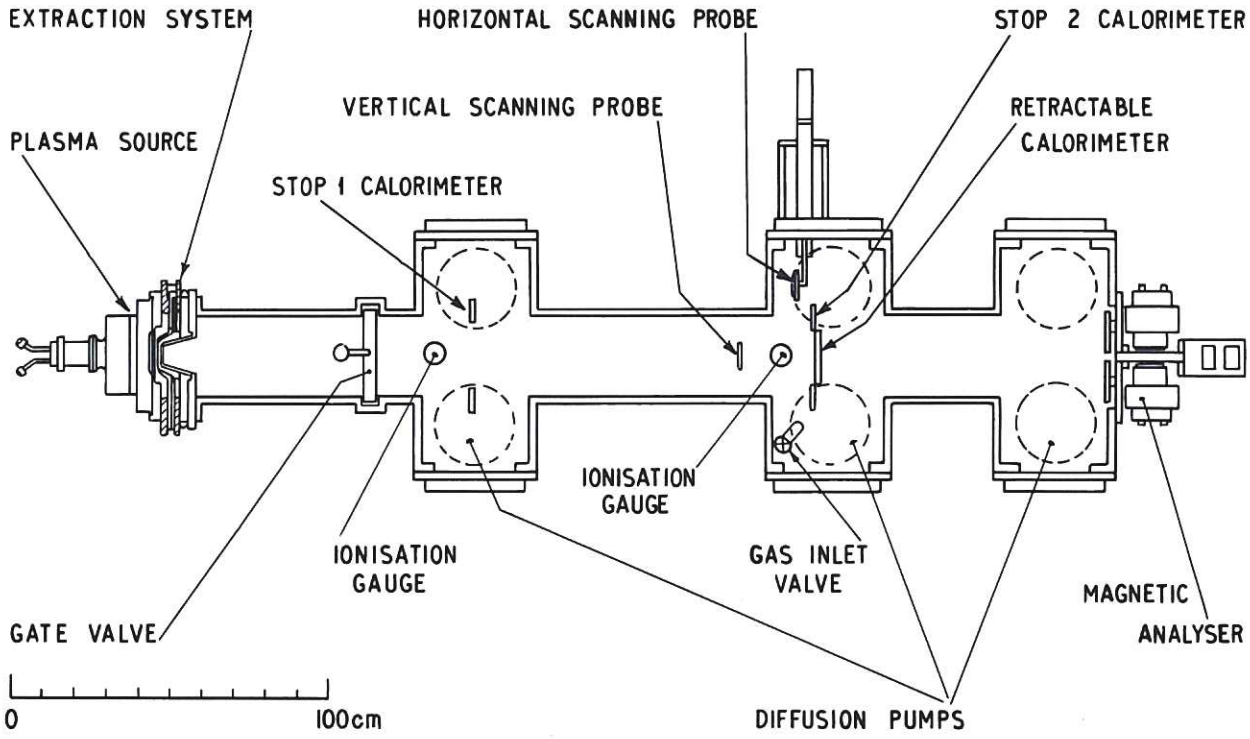

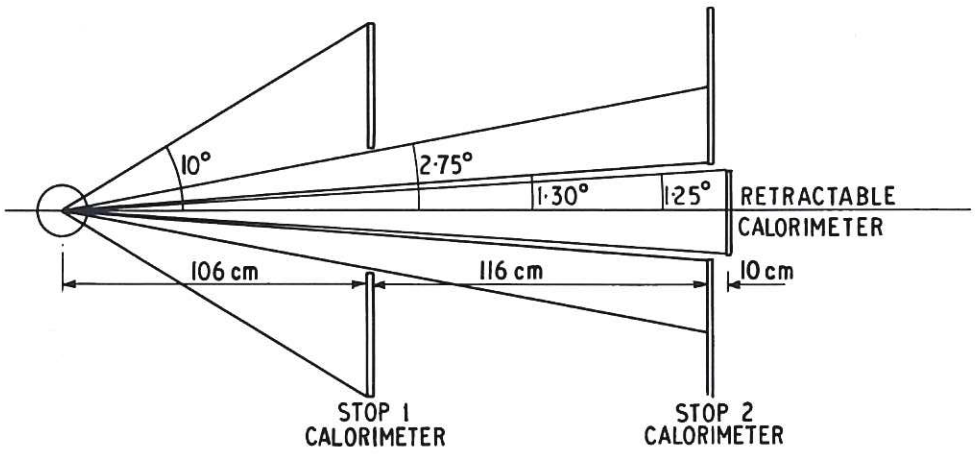

Fig.3 Upper: Beam flight path arrangement. Lower: Location of the three concentric calorimeters used to measure beam intensity within the angular ranges shown.

CLM-P 312

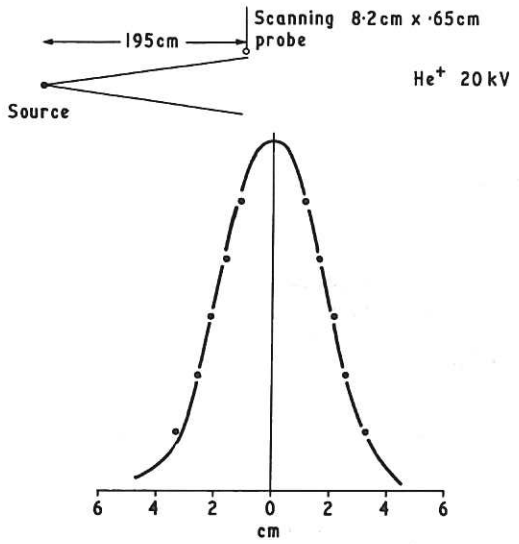

Fig.4 Beam profile obtained at 195 cm from the source (solid curve). A gaussian beam profile normalised at 0 cm was used to calculate the points (solid circles).

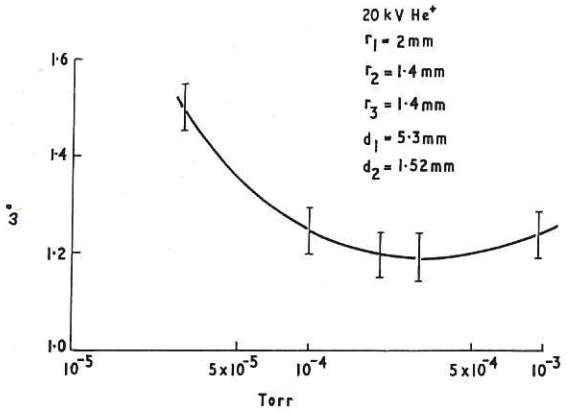

Fig.5 Variation of beam divergence ω with air pressure in the beam line.

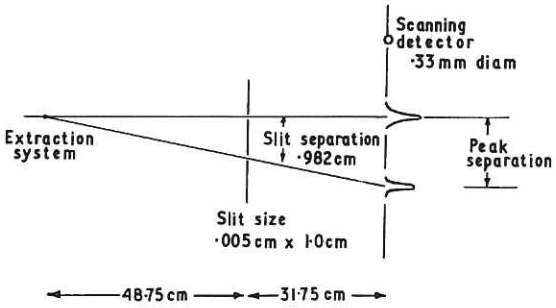

Fig.6 Arrangement of slits and scanning probe used to measure ion trajectories.

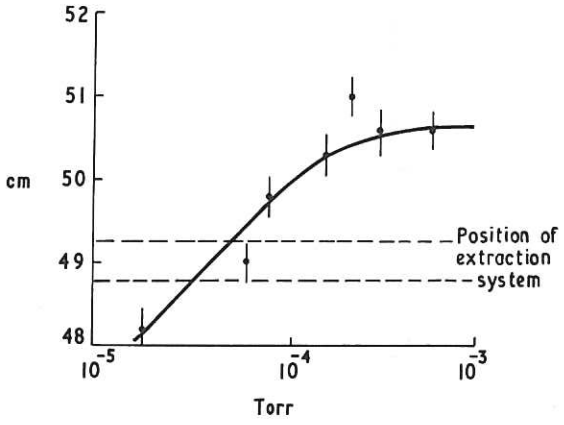

Fig.7 Location of apparent source point for ion trajectories as a function of air pressure in the beam line. Distances are relative to the plane of the two slits shown in Fig.6. Results are for 20 keV He^+ with r_1 = 1 mm, r_2 = r_3 = 0.7 mm, d_1 = 2.6 mm, d_2 = 0.8 mm and a recessed positive electrode as in Fig.22.

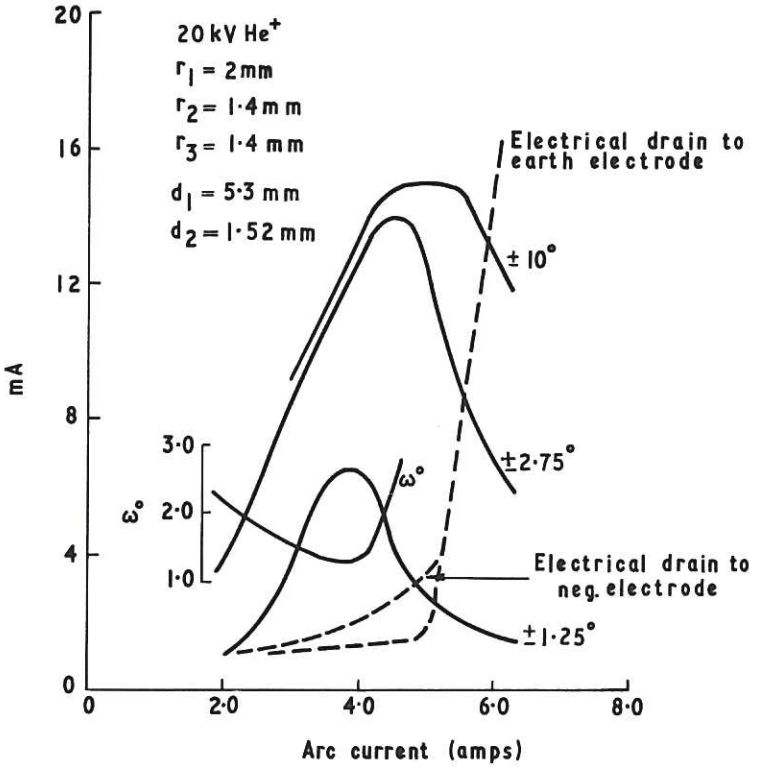

Fig.8 Variation of ion current within the angles indicated as a function of arc current (or plasma density) with all other parameters held constant.

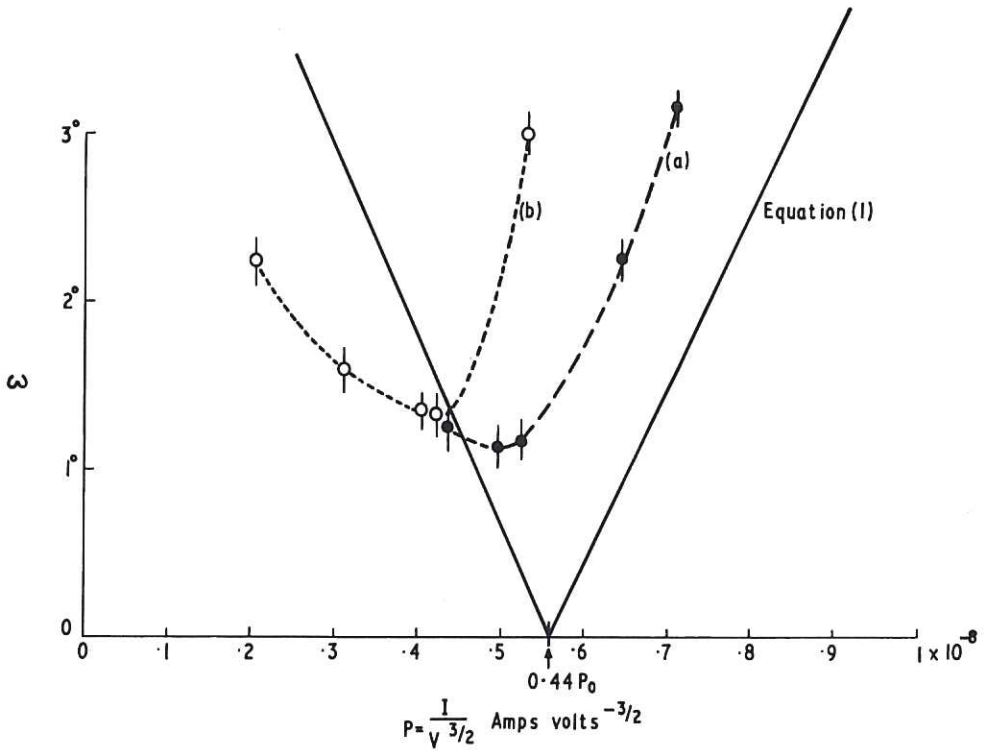

Fig.9 Variation of beam divergence ω as a function of perveance for a He^+ beam with I taken to be the total extracted ion current. The results were obtained in case (a) by varying V^+ and in case (b) by varying arc current while keeping all other parameters constant. In case (a) r_1 = 3 mm, $r_2 = r_3$ = 2.1 mm, d_1 = 7.6 mm and d_2 = 1.65 mm. In case (b) r_1 = 2 mm, $r_2 = r_3$ = 1.4 mm, d_1 = 5.3 mm and d_2 = 1.52 mm.

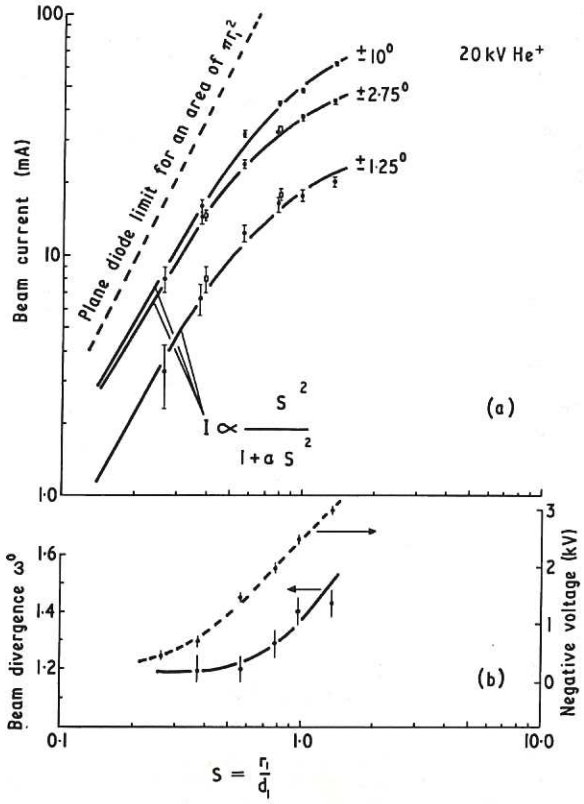

Fig.10 The maximum beam current available within the indicated angles is plotted as a function of the apsect ratios $S = r_1/d_1$. The solid curves are fitted to the experimental points. Here $r_2/r_1 = 0.7$, $r_3 = r_2$, $d_2/r_2 = 0.79$ to 1.1, open squares $r_1 = 3$ mm and solid circles $r_1 = 2$ mm. (b) The minimum beam divergence ω and optimum V- are shown as a function of S.

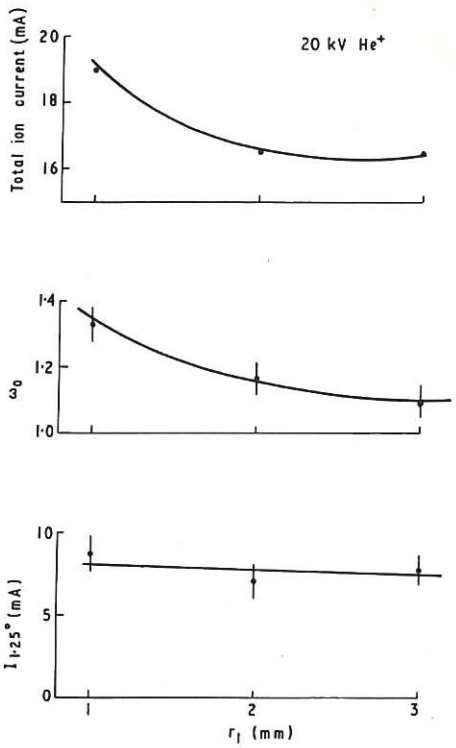

Fig.11 Variation of total ion current, beam divergence and maximum current within ±1.25° is plotted for three scale sizes, $r_1 = 1$, 2 and 3 mm. Here $r_2/r_1 = 0.7$, $r_3 = r_2$, S = 0.38.

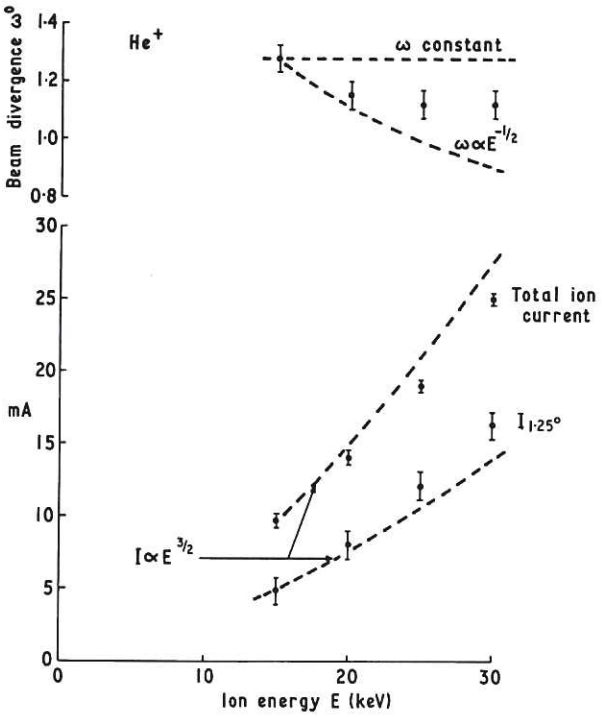

Fig.12 Variation of beam divergence and current with the beam energy. The $\omega \propto E^{-\frac{1}{2}}$ curve was fitted to the 15 keV result and corresponds to a transverse ion temperature of approximately 7 eV. Here r_1 = 2 mm, S = 0.38, r_2/r_1 = 0.7, $r_2 = r_3$ and d_2/r_2 = 1.1.

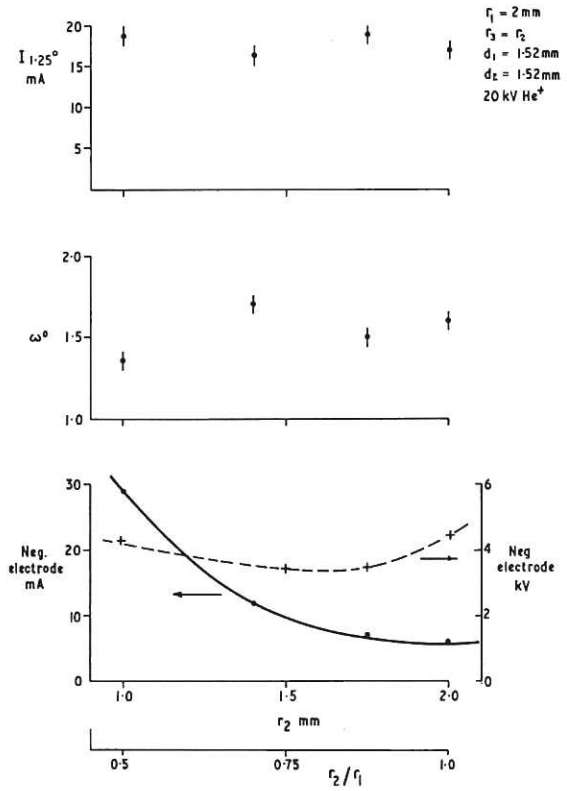

Fig.13 Dependence of beam current in ± 1.25° and divergence on radius of negative electrode aperture, r_2, to that of the positive, r_1, for S = 1.33. The lower curves show the V^- potential used and the current to the negative electrode.

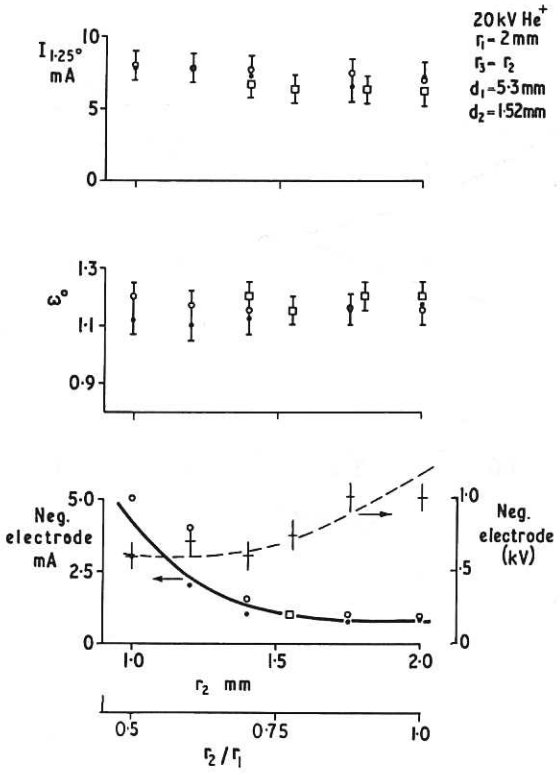

Fig.14 Dependence of beam current in ± 1.25° and divergence on radius of negative electrode aperture, r_2, to that of the positive, r_1, for S = 0.38. The lower curves show the V^- potential used and the current to the negative electrode. The various symbols represent data taken on different occasions.

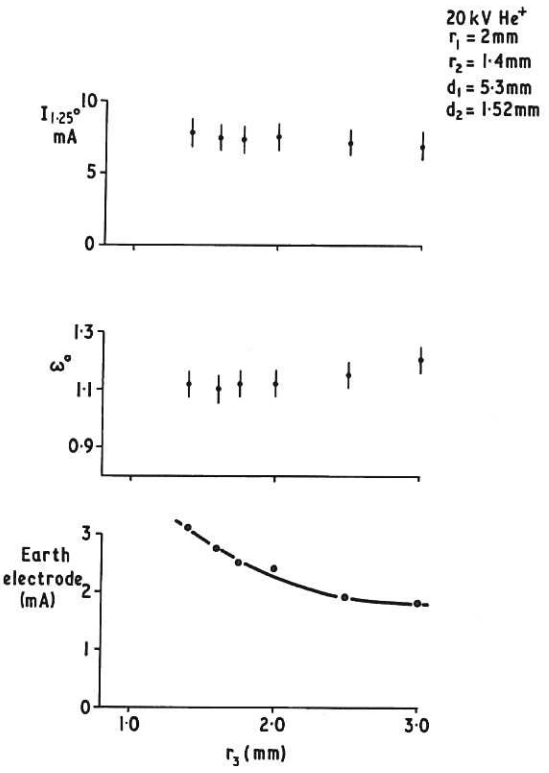

Fig.15 Variation of beam current in ± 1.25°, divergence and electrode current drain on the radius r_3 of the earth electrode aperture.

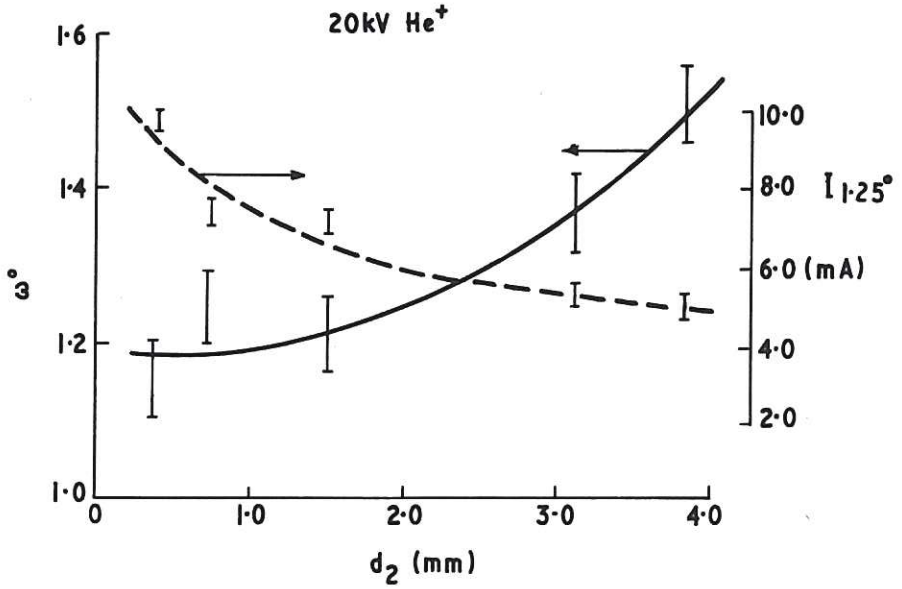

Fig.16 Variation of beam current in ± 1.25° and divergence on the length of the second gap, d_2. Here S = 0.38, r_1 = 2 mm, r_2/r_1 = 0.7, $r_2 = r_3$.

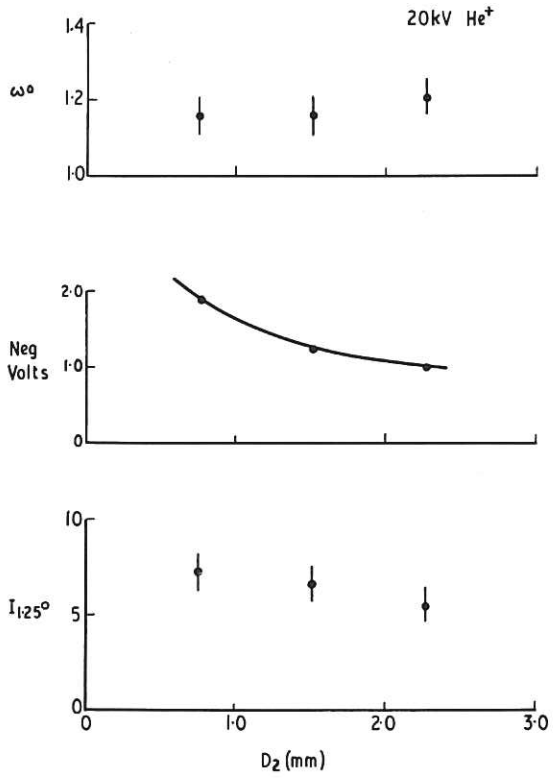

Fig.17 Variation of beam divergence, optimum V^- potential and current in ± 1.25° as a function of the thickness of the negative electrode D_2. Here S = 0.38, r_1 = 2 mm, r_2/r_1 = 1.0, $r_2 = r_3$ and $\frac{d_2}{r_2}$ = 0.75.

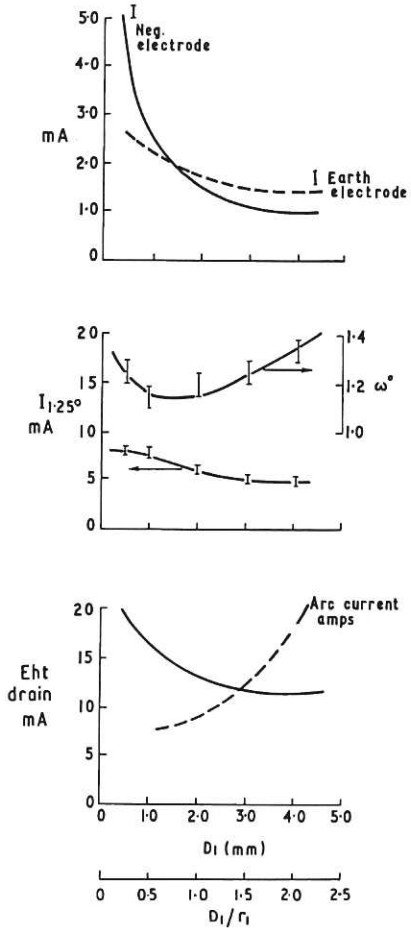

Fig.18 Variation in source performance as a function of the thickness of the positive electrode D_1. Here S = 0.38, r_1 = 2 mm, r_2/r_1 = 0.7, $r_2 = r_3$, d_2/r_2 = 1.1 and the results were obtained for a 20 keV He^+ beam.

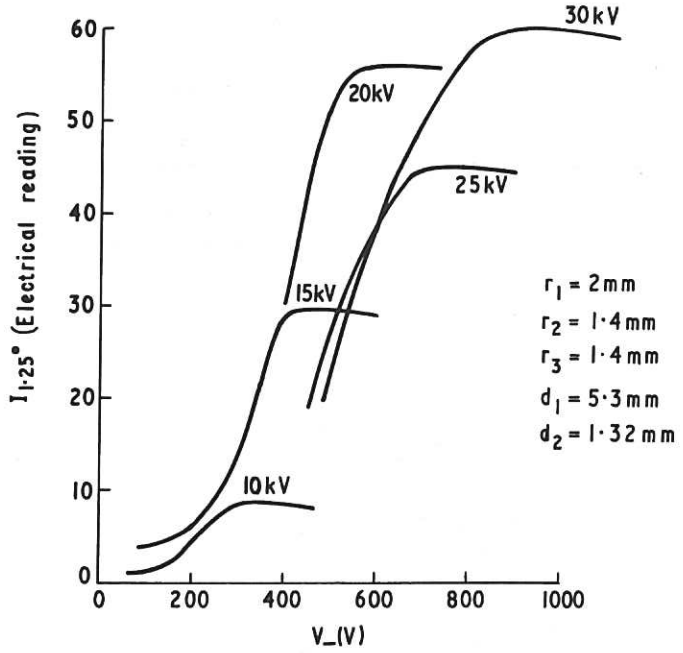

Fig.19 Change in beam current in ± 1.25° for low V^- potentials at five beam energies (V^+). The rapid increase in I occurs when V^- is strong enough to prevent the loss of electrons from the beam plasma by the V^+ potential. The current values for 10, 15 and 20 kV have been scaled for convenience.

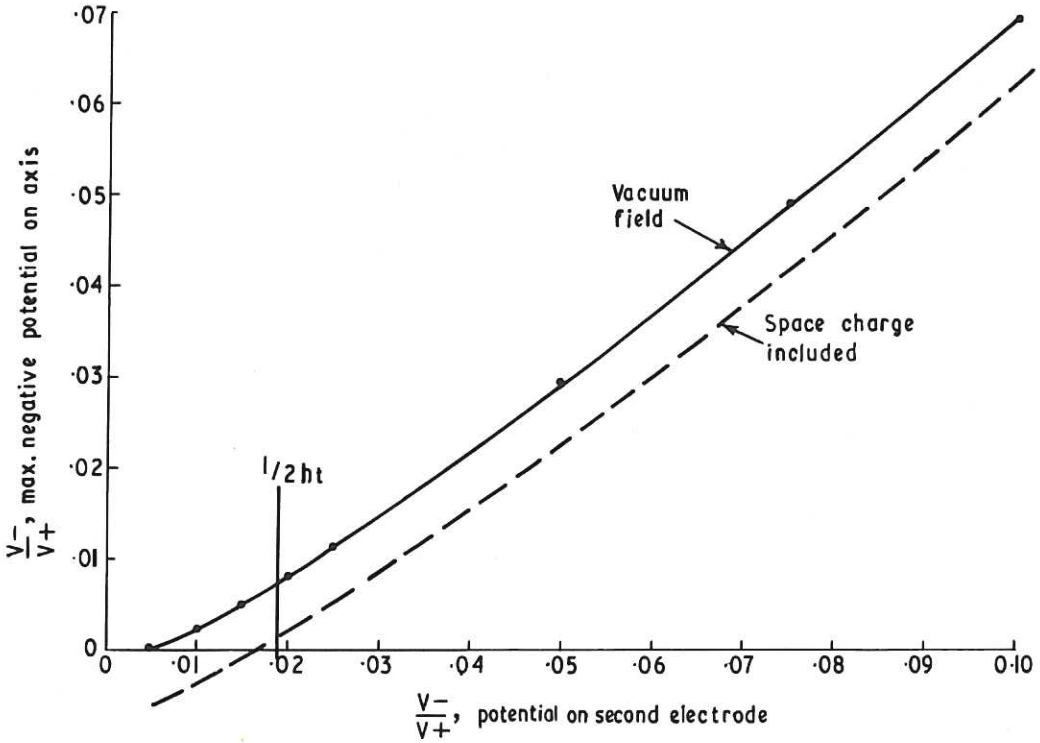

Fig.20 The solid curve shows the calculated negative potential on axis as a function of the applied V^-. The broken curve includes the effect of the beam space charge potential. The ratio of V^-/V^+ at half height of the results in Fig.19 is shown for comparison.

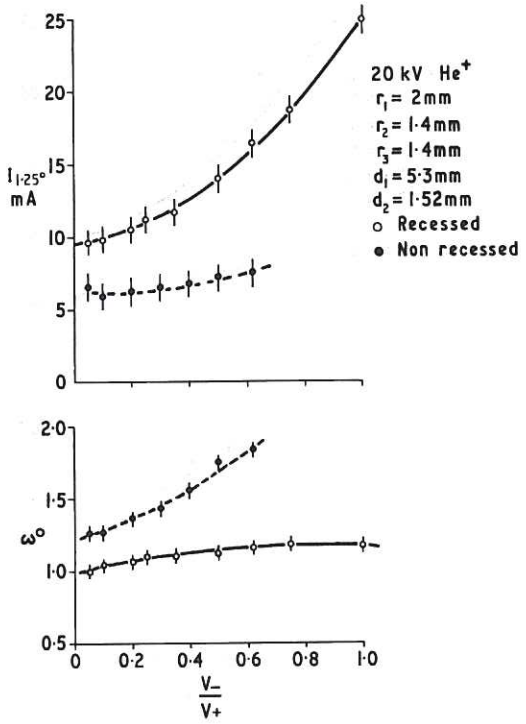

Fig.21 Variation of beam current in ± 1.25° and divergence as a function of V^-/V^+ at constant V^+. Solid circles are for a non-recessed positive electrode as in Fig.2 and open circles are for a recessed electrode as shown in Fig.22.

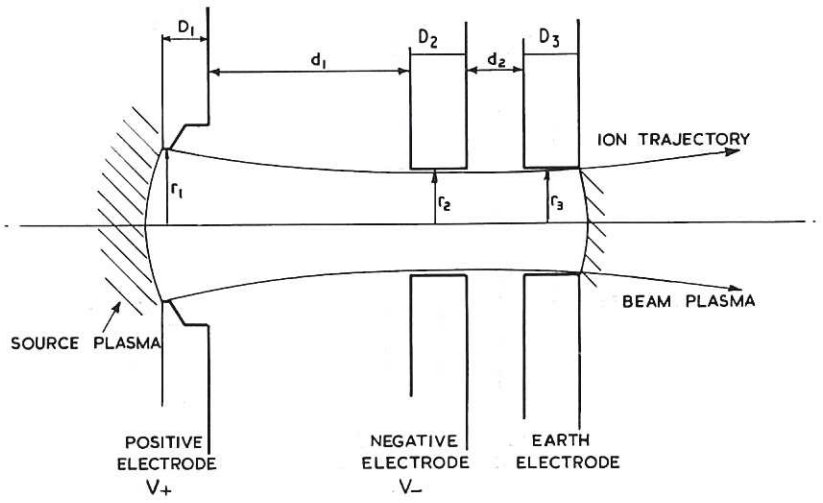

Fig.22 The single aperture electrode system with recessed positive electrode as used by Cooper et al[7].

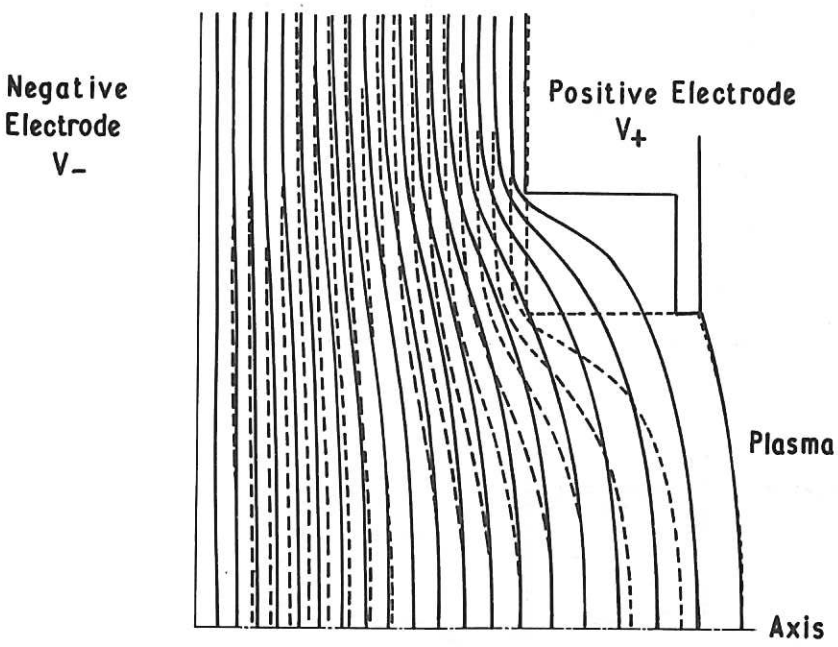

Fig.23 Vacuum field equipotentials computed for recessed (solid lines) and non-recessed (broken lines) positive electrodes.

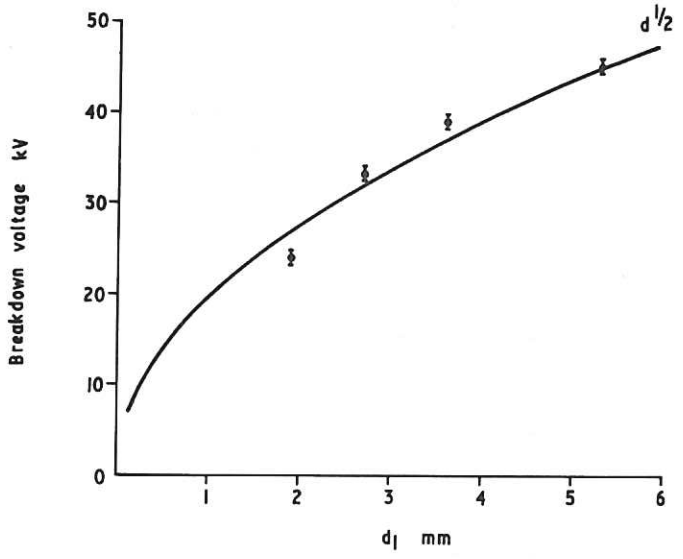

Fig.24 Variation of the potential $V_T = V^+ + |V^-|$ at which some breakdowns were experienced is shown as a function of the first gap length d_1. The solid curve assumes a relation of the form $V = B\, d_1^{\frac{1}{2}}$ with $B = 6 \times 10^3$ volt. $cm^{-\frac{1}{2}}$.

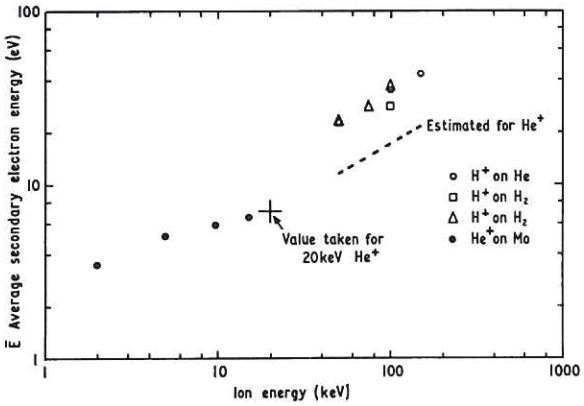

Fig.AI.1 Average energy of electrons ejected in collisions between ions and gas molecules and between ions and a metal surface. Open circles and squares are taken from ref.(24), open triangle from ref.(23) and solid circles from ref.(22).

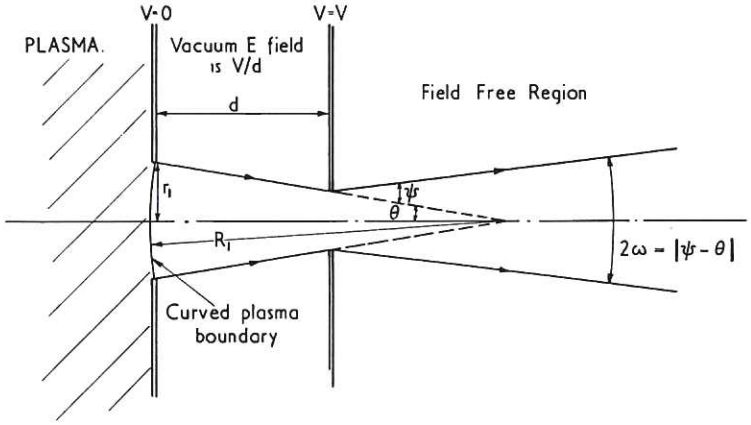

Fig.AII.1 Scheme of simplified ion optics in beam extraction region.

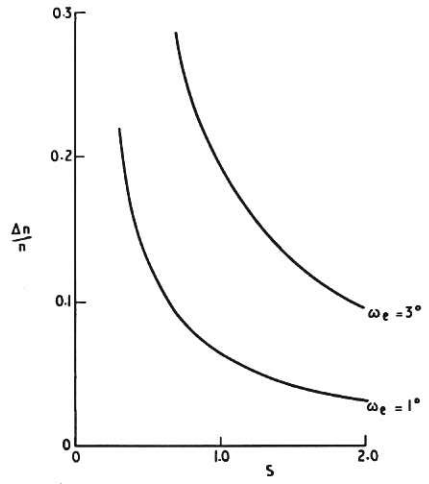

Fig.AIII.1 Variation of limiting value of $\Delta n/n$ with aspect ratio S for beam divergence of 1° and 3°.